Available online at www.sciencedirect.com
ScienceDirect
Journal of Power Sources 160 (2006) 326–333
JOURNAL OF POWER SOURCES
www.elsevier.com/locate/jpowsour

The influence of catalyst layer morphology on the electrochemical performance of DMFC anode

Zhanliang Wang *, Yang Liu, Vladimir M. Linkov

South Africa Institute for Advanced Material Chemistry, Department of Chemistry, University of the Western Cape, Private Bag X17, Bellville, 7535 Cape Town, South Africa

Received 29 November 2005; received in revised form 11 January 2006; accepted 13 January 2006
Available online 28 February 2006

Abstract

The anodes with different morphology for DMFC were prepared, and the influences of the microstructure of anode catalyst layer on their electrochemical performance were investigated by scanning electrochemical microscopy (SECM), scanning electron microscopy (SEM), proton induced X-ray emission (PIXE) and electrochemical methods, respectively. The surface morphology of catalyst layer was observed by SEM, and the elements dispersion status and its distribution of activity intensity on electrode catalyst layer were mapped by PIXE and SECM, respectively. Electrochemical impedance spectroscopy (EIS) and anode polarization experiment were employed to analyze the electrochemical properties of anode. The results reveal that the anode with a relative smooth surface of catalyst layer and less cracks shows good interfacial properties and the lower resistance on the electrode reaction of methanol, and its maximum power of MEA as a single cell was about 178 mW cm^{-2} at 70 °C.

Keywords: DMFC; Catalyst; SECM; EIS

1. Introduction

In recent years, direct methanol fuel cell has attracted intensive research interests because of its high power density and efficiency, zero emission and reliability. Nevertheless, further improvements on the performance of the DMFC are required before it can be widely utilized in a practical application. As we known, there are two most serious technical obstacles restricting its development of DMFC. One is methanol crossover to the cathode through proton conductive polymer membrane, and another is the catalyst's poisoning caused by the intermediates of methanol oxidation. Great efforts have been concentrated on the researches about carbon monoxide tolerant catalysts [1–3] and low methanol permeability polymer electrolyte membranes [4,5]. It is a challenging problem to develop stable anode catalyst with high electro-catalytic activity in the approach of DMFC commercialization. So far, Pt–Ru alloys supported on carbon with high surface area are considered as the best catalysts for methanol oxidation reaction.

In terms of the characterization method of electrocatalysts, particle size, active surface area of catalysts, and kinetics parameters are usually measured by transmission electron microscopy (TEM), cyclic voltammetry, EIS and Tafel plot, respectively [6–8]. The information obtained from these parameters reflects the properties of electro catalyst in nature. However, these natural properties of catalyst are only part of the factors that determine the performance of electrode in a single cell. The approach to the preparation of electrode usually used is to form catalyst layer on gas diffusion layer by coating inks composed of catalyst, ionomer and solvent onto the conductive substrate such as carbon fiber cloth or carbon paper. The microstructure of catalyst layer can affect the mass transfer of reactant and product, and then influence the electrochemical reaction rate. So, the microstructures of catalyst layer together with the natural properties of catalyst determine electrochemical performance of electrode. The main requirement for a good catalyst layer is the maximized triple-phase boundary, where the electrochemical reaction takes place. Many works [9–12] have been done to investigate the influences of microstructure, composition and gas diffusion layer on the discharge ability of electrode. Among of them, it is a typical route to investigate the surface and cross-section morphology using scanning electron microscopy [13].

* Corresponding author. Tel.: +27 21 9593080; fax: +27 21 9593080.
E-mail address: zlwang2k2@yahoo.com (Z. Wang).

0378-7753/$ – see front matter © 2006 Elsevier B.V. All rights reserved.
doi:10.1016/j.jpowsour.2006.01.056

Physical structure such as pore diameter and distribution in catalyst layer can be observed through SEM images. But the electrochemical properties including electro-catalytic activity intensity and active sites distribution on the surface of electrode can't be described visually by SEM image. The influence of surface morphology of electrode on the cell performance is still unclear.

In order to investigate the relationship between morphology of catalyst layer and electrochemical behaviors, three types of anode were prepared and investigated by SECM, PIXE and diversified electrochemical methods in this paper. SECM is a versatile tool for the characterization of catalyst, which can be utilized to mapping the catalysis activity of catalyst along the surface of electrode [14–16]. SECM and PIXE were employed to observe the topography and the distribution of active elements on the anode catalyst layer, respectively. SECM images reflect the electrochemical information related to the electro catalysis activity intensity and active sites distribution of the catalyst layer. Ru distribution status in catalyst layer was measured by particle induced X-ray emission. An equivalent circuit was proposed to analyze the EIS results of anode, and the experimental values can be well fitted by this equivalent circuit.

2. Experimental

2.1. Chemicals

Commercial Vulcan XC-72, hydrogen hexachloroplatinate ($H_2PtCl_6{\cdot}6H_2O$, Aldrich), ruthenium chloride ($RuCl_3$, Aldrich), formaldehyde (Aldrich), isopropanol (99%, Aldrich), PTFE emulsion (60%, Aldrich) and Nafion solution (5 wt.%, Ion Power Inc.) were used as-received. Nafion 117 membrane (1100 EW, Ion power Inc.) was treated with 5% H_2O_2 and 1 mol L^{-1} H_2SO_4 as reference method [17] prior to use. Carbon cloth (type A, E-TEK) was used as conductive substrate for electrode. A mixture of Vulcan XC 72 carbon black and 20% dry weight PTFE emulsion was coated on the carbon cloth using a doctor blade to form a microporous layer. The coated carbon cloth was dried in an oven at 100 °C for 20 min and then at 330 °C for 30 min. Solutions were made with ultra-pure water (17 M, Millipore).

2.2. Preparation of Pt–Ru/C catalyst and of electrode

Pt–Ru/C catalyst was prepared by liquid-phase reduction of chloroplatinic acid and ruthenium chloride with formaldehyde. An aqueous solution containing chloroplatinic acid and appropriate amount of ruthenium chloride (Pt:Ru = 2:1 in weight) were mixed with carbon black and allowed for complete impregnation. Then, formaldehyde was dropped into the suspension as fast as possible. The resultant mixture was maintained at 80 °C for 3 h to allow complete reduction of Pt and Ru. Subsequently, the mixture was filtered and washed with de-ionized water to remove chloride ions. The catalyst was dried in an oven at 80 °C until to a constant weight.

Ink was made by mixing 80 wt.% Pt–Ru/C, 15 wt.% Nafion solution, 5 wt.% PTFE and isopropanol with ultrasonic bath. Then, electrodes were obtained by two methods including spraying ink onto carbon cloth with airbrush gun and spreading ink onto carbon cloth with brush. The electrodes made with brush and spray gun were denoted as BE and SE, respectively. RE represented the electrode obtained by treating SE with roller. Pt–Ru loadings for all the three anodes were about 1.5 mg cm^{-2}. Commercial Pt/C catalyst (40 wt.% Pt, Alfa, Asear) was made into cathode using the same method as anode RE, and Pt loading was 1.2 mg cm^{-2}. Membrane electrode assembly (MEA) was prepared by hot-pressing electrodes on pre-treated Nafion membrane at 135 °C under a load of 10 MPa for 2 min.

2.3. Measurements

The nanomorphology of the supported catalysts was observed by transmission electron microscopy (TEM) using a LEO 910 microscope. The sample for the TEM analysis was prepared by ultrasonically treating the catalyst powders in the mixture of water and isopropanol. One drop of the suspension was applied onto clean holey copper grids and dried under infrared lamp. The X-ray diffraction (XRD) pattern for the catalyst was obtained using a D8 Discover (Bruker AXS, German) X-ray diffractometer with the Cu Kα radiation source.

Rotating disc electrode was used to characterize the electrochemical properties of Pt–Ru/C catalyst. Five milligrams of Pt–Ru/C catalyst was suspended in 1 mL of isopropanol and 50 μL of Nafion solution to prepare catalyst ink. Then 25 μL of ink was coated onto the surface of a clean glassy carbon disk electrode with an area of 0.078 cm^2. The electrode was dried at 80 °C for 10 min to remove isopropanol. A mixture solution containing 1 mol L^{-1} H_2SO_4 and 1 mol L^{-1} methanol was used as electrolyte. Cyclic voltammetry experiments were carried out on Autolab (PGSTATE30, ECO-CHEMIE) at ambient temperature (25 °C). Saturated calomel electrode (SCE) was used as reference electrode, and platinum wire as auxiliary electrode. Scan rate for cyclic voltammetry was 25 mV s^{-1}.

SECM was applied to investigate topography of electrode, and the measurement was carried out with SECM 270 (Uniscan Instrument Ltd., UK). A 25 μm diameter Pt-UME (ultra microelectrode) was used as the SECM tip, while electrode containing Pt–Ru/C as the substrate was sealed at the bottom of Teflon cell. Auxiliary and reference electrodes were Platinum coil and Ag/AgCl, respectively, and 5 mmol L^{-1} mM sulphuric acid served as electrolyte. The microscope was configured to scan an area of 1000 μm × 1000 μm at a tip-substrate distance of 5 μm. The substrate was kept at a potential of 0 V, and a potential of −1.2 V (mass transport limited region for proton reduction) was applied to the tip to reduce H^+.

Surface morphology of electrodes was observed by scanning electron microscopy (HITACHI X-650). Distribution of Ru in electrode catalyst layer was observed by PIXE. Sampling areas were selected as 1000 μm × 1000 μm (X:Y). Samples were irradiated with 3.0 MeV protons. K-shell X-ray excitation was used for Ru content analysis.

Anode polarization curves were measured by galvanodynamic polarization mode with a scan rate of 1 mA s^{-1} at 70 °C. One mole per litre methanol solution fed to the anode at 1 mL min^{-1} served as working electrode, and humidified hydro-

gen was fed to cathode chamber at 50 mL min^{-1} with zero back pressure, which was acted as counter electrode and reference electrode (dynamic hydrogen electrode, DHE). The impedance spectra were carried out at frequencies between 100 kHz and 10 mHz under the same conditions as anode polarization experiments. The performance of MEA as a single cell was tested on fuel cell testing station (Lynntech Inc.) with 2 mol L^{-1} methanol solution at flow rate of 1 mL min^{-1} and 1 bar oxygen gas at the rate of 50 mL min^{-1}. The experiment was carried out at 70 °C.

3. Results and discussion

3.1. Characterization of catalyst

Fig. 1 shows the TEM image of the home-made Pt–Ru/C catalyst. As can be seen the distribution of the particles of Pt–Ru is homogenous on the XC-72 carbon support and the catalyst is well dispersed. The average particle size calculated from the TEM analysis is about 3.3 nm. Fig. 1(b) gives the XRD pattern of the home-made Pt–Ru/C catalyst. The XRD pattern clearly shows the four characteristic peaks, which are corresponding to the (1 1 1), (2 0 0), (2 2 0) and (3 1 1) crystal faces of face centered cubic (fcc) crystalline Pt, respectively. No obvious peak for Ru is observed in Fig. 1(b), which means that the alloy catalyst resembles the single-phase disordered structure (solid solution).

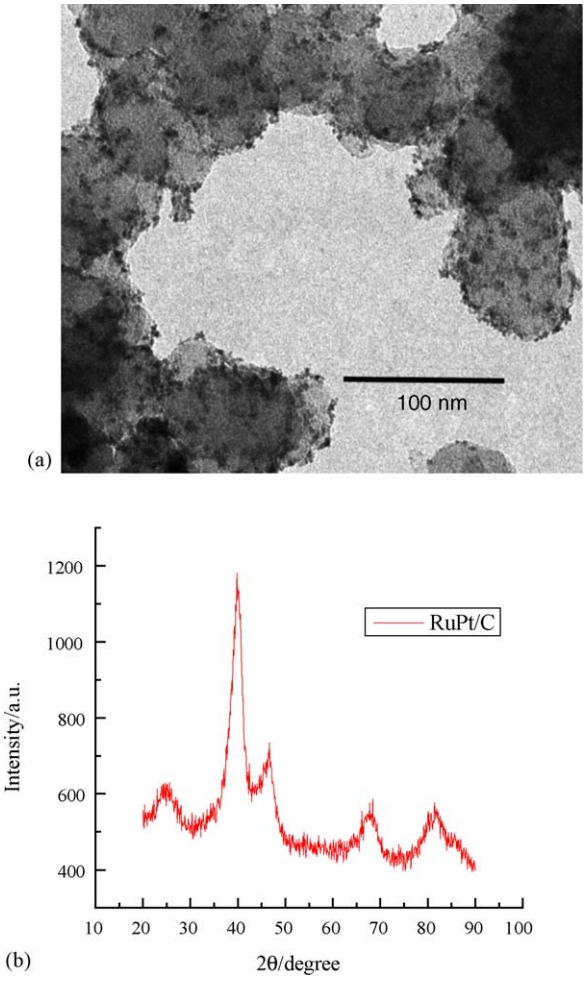

Fig. 1. (a) TEM image of Pt–Ru/C catalyst. (b) XRD pattern for home-made Pt–Ru/C catalyst.

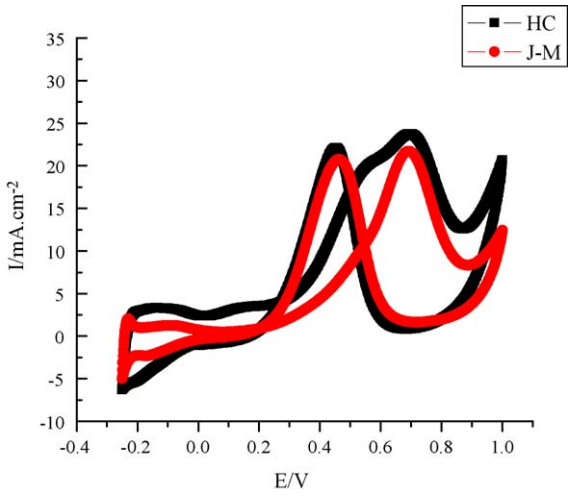

Fig. 2. Voltammogram of Pt–Ru/C in 1 mol L^{-1} methanol and 1 mol L^{-1} H_2SO_4 mixture.

To investigate the catalytic activity of Pt–Ru/C, cyclic voltammetry experiment was carried out. Fig. 2 shows the voltammograms of home-made Pt–Ru/C (denoted as HC) and commercial Pt–Ru/C catalyst (Pt 10 wt.%, Ru 20 wt.%, J–M, purchased from Johnson Matthey company) in 1 mol L^{-1} methanol and 1 mol L^{-1} H_2SO_4 mixture solution, which were cycled from −0.25 to 1.0 V at the scan rate of 25 mV s^{-1}. It can be seen that two peaks, which are related to the oxidation reaction of methanol and the corresponding intermediates produced during the methanol oxidation, appear at about 0.69 and 0.44 V for both home-made catalyst and commercial catalyst, respectively. The forward and the backward peak current density are about 23.9 and 22.1 mA cm^{-2}, respectively, which are slightly higher than those of J–M catalyst. Compared with J–M catalyst, the forward peak for home-made Pt–Ru/C is more broad, which means that home-made catalyst can deliver higher reaction current at same potential than that of J–M catalyst.

3.2. Microstructure of electrode

Fig. 3(a)–(c) show the SEM images of the anode catalyst layer prepared by three different methods. Fig. 3(a) shows the surface morphology of anode BE. It can be seen that many cracks with the size of 5–10 μm distribute on the surface of catalyst layer, In contrast to the morphology of anode BE, the catalyst layer of electrode SE, as shown in Fig. 3(b), has few cracks. However, its surface of catalyst layer is uneven because of catalyst agglomerates. The difference of the surface morphology can be ascribed to the volume shrinkage of catalyst layer. The solvent evaporation velocity in brushing method is relatively slower than that of spraying method. During spreading ink with a brush, the solvent always soaks the catalyst layer formed on the carbon paper

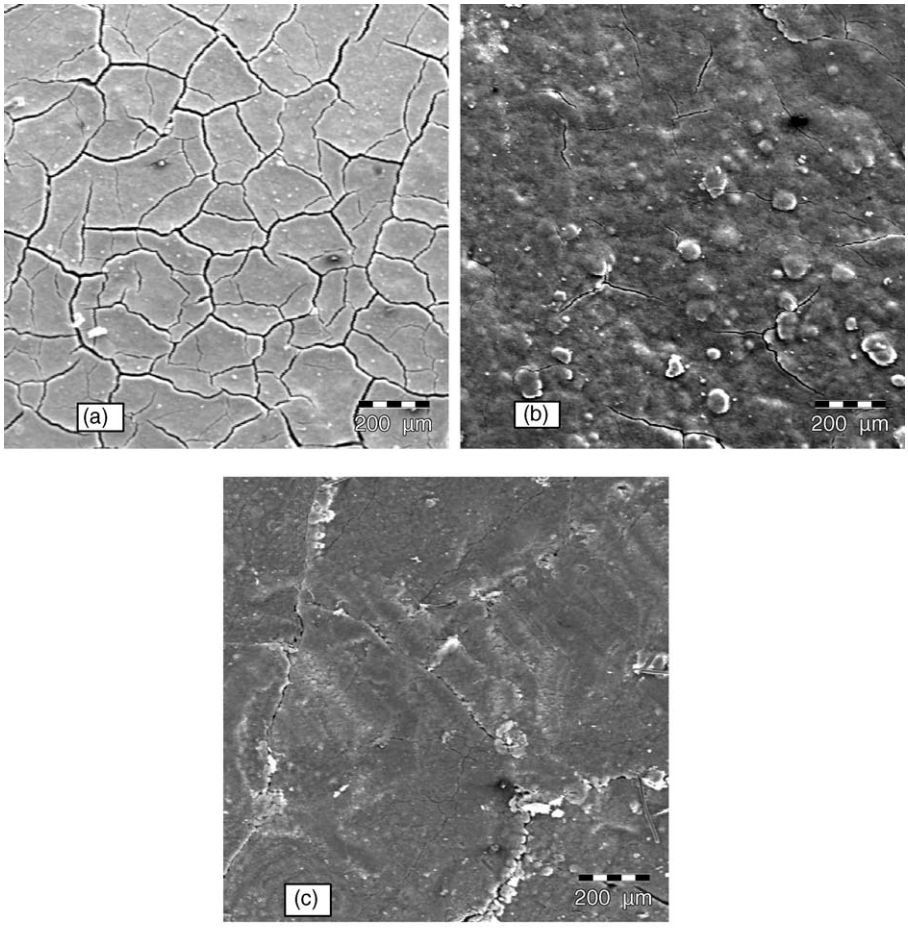

Fig. 3. SEM micrographs of: (a) surface of anode BE, (b) surface of anode SE, and (c) surface of RE.

by previous brushing process. The catalyst layer is very thick since a high catalyst loading is necessary for direct methanol fuel cell. Mud-cracking takes place on the catalyst layer due to the apparent volume shrinkage of the catalyst slurry after the solvent evaporation. As far as spraying method is concerned, the ink can be sprayed on the surface of carbon paper uniformly, and most of the solvent can evaporates quickly before soaking the dry catalyst layer existing on carbon paper. Therefore, the volume change in catalyst layer of anode SE is smaller than that of BE. In order to obtain a flat and smooth catalyst layer, the electrode RE was prepared by rolling anode SE. As can be seen in Fig. 3(c), most of the cracks and big size particles on the surface of RE disappear. This planar surface is supposed to form better interfacial contact between catalyst layer and polymer ionic conductor (Nafion 117).

Fig. 4(a) and (b) show the high magnification surface image and cross-section image of anode RE, respectively. It can be seen that the catalyst layer has a rich porous structure, and the pore size mainly distributes in the range of 0.1–0.5 μm. The observed pores in Fig. 4 are generally assigned to the secondary pores, which are relative large pores. According to the Refs. [12,18], the microstructure of catalyst layer composed of the primary pores and the secondary pores. The primary pores with a size range less than 0.1 μm form within the agglomerates, while the secondary pores are between the agglomerates. The inner surface of the pores is the main catalyst/ionomer/reactant interface, where the electrochemical reaction takes place. The reactant (methanol solution) transports to the reaction interface only through the primary pores and the secondary pores. Therefore, the pore size distribution of the primary pores and secondary pores influence the reactant transfer process and active surface area, and then affect the electrochemical performance of electrode. In next subsection, the relationship between surface morphology of anode and electrochemical properties will be discussed.

The distribution of catalytic activity sites on the surface of catalyst layer can be observed from a SECM image, which was obtained by monitoring the local proton electrochemically generated at substrate (Pt–Ru/C on carbon paper). Fig. 5(a) and (b) show the typical SECM image of anode SE and of anode RE. The SECM images exhibit the current changes along the horizontal coordinates. In the scanned region of 1000 μm × 1000 μm, the responding current through the probe changes from 0 to 10 nA for both anode SE and anode RE. Compared to anode SE, the current intensity distributes more uniform on anode RE. The topography image of anode for DMFC mapped by SECM visualizes the distribution of catalytic activity sites on the surface

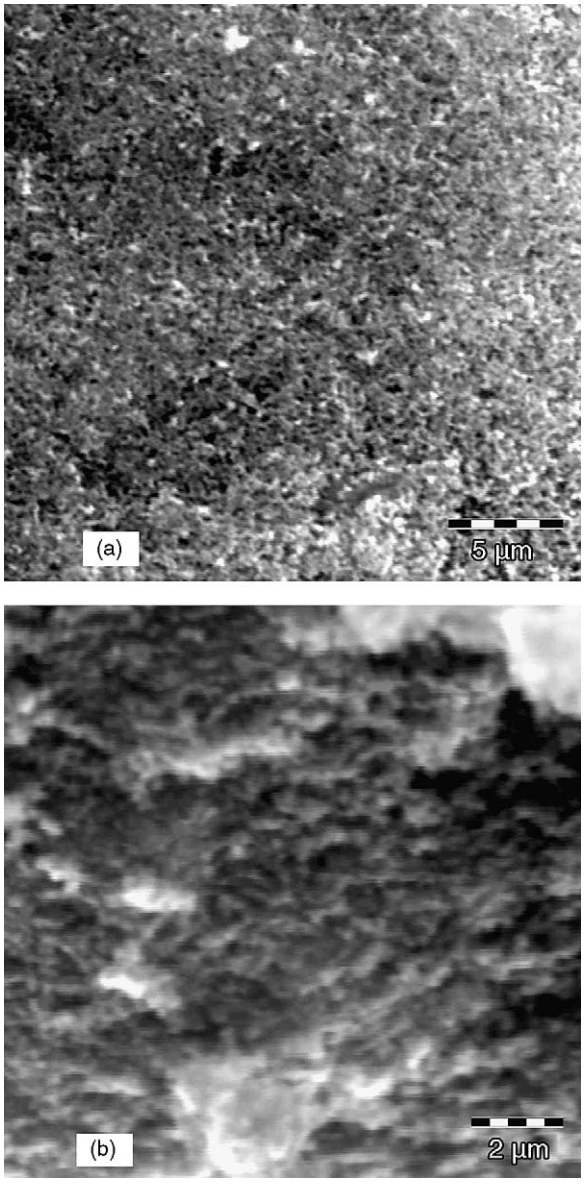

Fig. 4. SEM images of: (a) surface of anode RE, and (b) cross-section of anode RE.

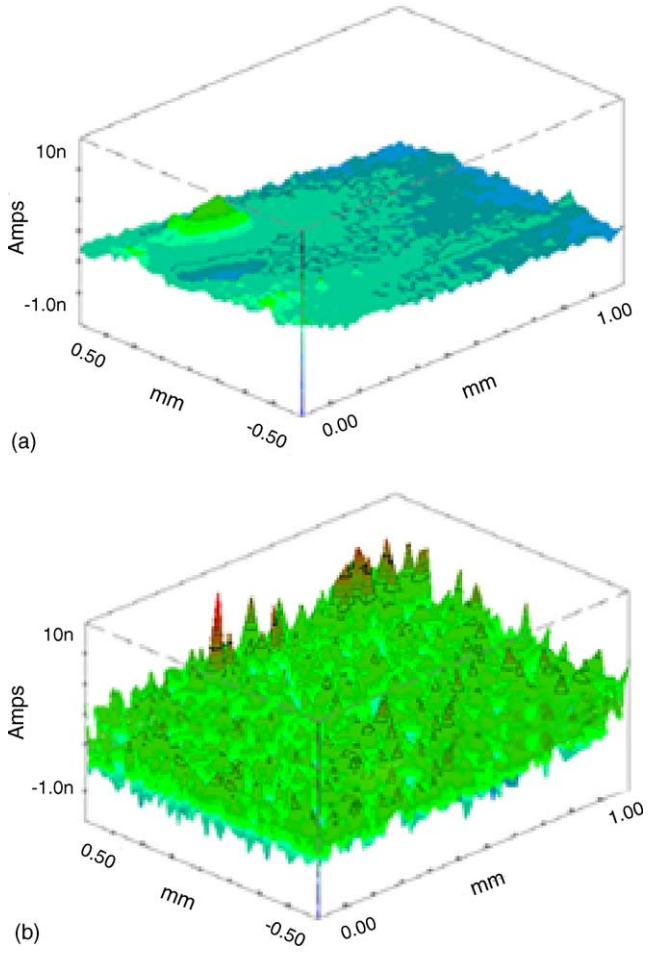

Fig. 5. Topographical images of: (a) anode RE, and (b) anode SE.

of electrode and can reflects its current distribution in MEA. To some extent, SECM image also provides the information on physical status of catalyst layer. Generally, only a homogeneous catalyst layer of electrode with a smooth and flat surface can form the map of electro-catalytic activity with well-distributed sites, which is beneficial for improving the performance and durability of MEA. The electro-catalytic activity of substrate and the distance between the tip and the substrate are two important factors determining the current response on the tip. The resolution of SECM in this experiment was set at 1 μm × 1 μm. Since the particle size of the catalyst Pt–Ru/C is only about 30 nm, the number of the Pt–Ru/C particles is so great in the area unit of 1 μm × 1 μm that the electro catalysis of Pt–Ru/C catalyst can be assumed to be uniform. From this point, the former factor is negligible for the current change through the tip. In this experiment, the tip was kept at a constant height relative to the substrate. Therefore, the fluctuation of current detected by the tip can be ascribed to the change of real distance between the tip and electrode surface, which is caused by the uneven catalyst layer surface. The SECM image is consistent with SEM result mentioned above. According to Fig. 4(a), the surface of catalyst layer comprises cavities and agglomerates formed by the mixture of catalyst and ionomer. The surface of catalyst layer is uneven in micron scale. These cavities, which are reflected in the low active metal content region of PIXE image, are supposed to be the low electro-catalytic activity region in SECM image. The PIXE images for the dispersions of Ru in the anode SE and RE are given as Fig. 6(a) and (b), respectively. PIXE results depict that the content of Ru is about 4%, and a large weight contribution from carbon, accounting for up to about 88% of the total weight. This is a mixed consequence of carbon contributions from the carbon as support material of the Pt/C catalyst and the carbon of the carbon cloth. Moreover, the PIXE results indicate that the dispersion of active elements is inhomogeneous in the magnitude of micron and the rich Ru (Ru and Pt alloy) regions form islands. That is caused by inhomogeneous distribution of Pt–Ru/C particle in the catalyst layer because of cracks and cavities. Since the electro catalysis activity of electrode strongly depends on the dispersion of active metal of the catalyst layer, these islands deliver good electrochemical activity than other

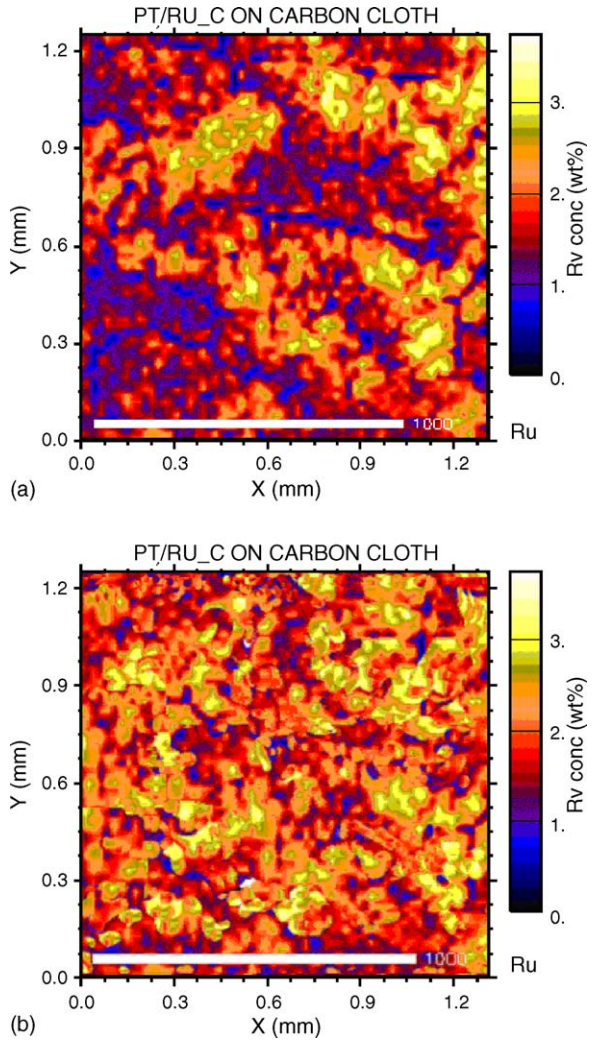

Fig. 6. PIXE images of Ru dispersions: (a) on anode SE, and (b) on anode RE.

regions. So the islands in PIXE image are corresponding to the high current intensity region in SECM image.

3.3. Electrochemical performance of anode with different surface morphology

Fig. 7 displays the anode polarization curves of MEAs with different anodes. The difference of electrochemical performance can be ascribed to the factor of anode since the polarization of DHE is negligible. The polarization potential decreases in the following order: BE > SE > RE. The MEA with anode RE delivers the best performance, and the current density at the anode potential versus DHE of 0.5 V is about 460 mA cm^{-2}. The polarization potential of MEA with anode BE shifts in positive direction dramatically with the current density increase. The performance difference of MEAs can be analyzed basing on the electrochemical reaction process. According to the electro-oxidation mechanism of methanol, electro-oxidation reaction of methanol takes place and produces proton, electron and carbon dioxide when methanol transfers to the interface of catalyst and ionomer through pores in the catalyst layer. Proton and electron

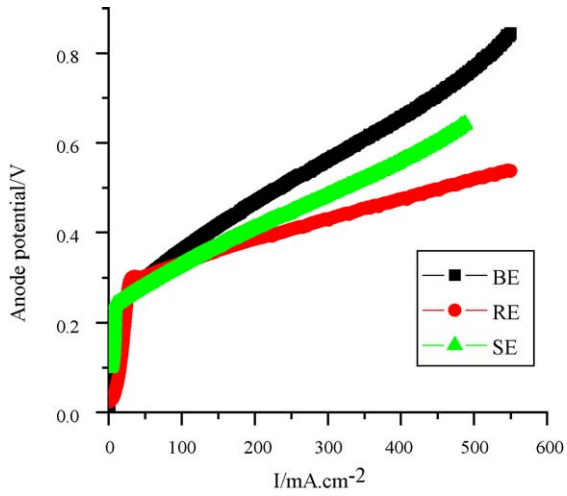

Fig. 7. Polarization curves of anodes with different surface morphology.

conduct through ionomer network and catalyst, respectively, and carbon dioxide escapes to outside through micro porous structure. In terms of the reaction rate, the electron transfer process or the mass transfer process including methanol and carbon dioxide may become the rate-determined step for anode electrochemical reaction. Generally, the reaction rate is controlled by the electron transfer process at low current region and by the mass transfer step at strong polarization region, respectively.

Fig. 8(a) shows an equivalent circuit for the anode AC impedance analysis. R_1 is the cell resistance. R_2 and C_2 represent the diffusion resistance of the methanol and the capacitance of

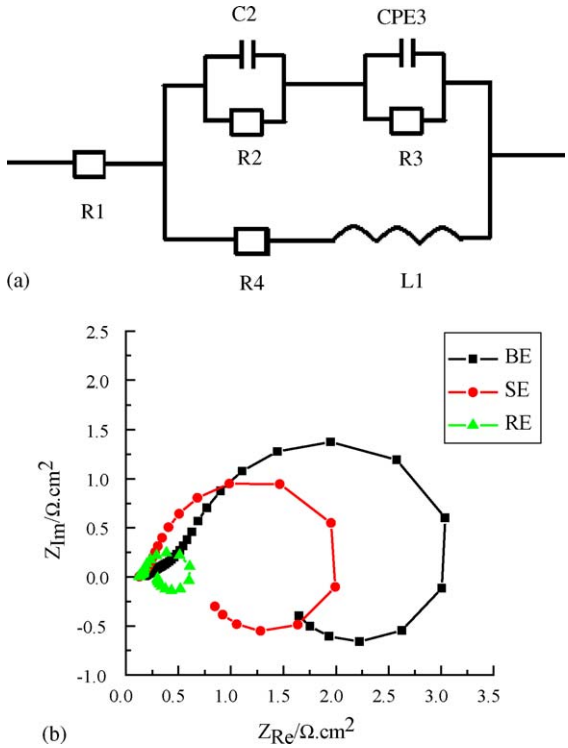

Fig. 8. (a) Equivalent circuit for the anode impedance analysis. (b) EIS of different anodes.

Table 1
Impedance parameters of MEA with various anode electrodes

Electrode	R_1 ($\Omega\,cm^{-2}$)	R_2 ($\Omega\,cm^{-2}$)	R_3 ($\Omega\,cm^{-2}$)	R_4 ($\Omega\,cm^{-2}$)
BE	0.168	3.05	0.769	2.08
SE	0.127	2.21	0.530	0.839
RE	0.125	0.40	0.313	0.253

the adsorption. R_3 and CPE_3 are the charge-transfer resistance at the interface of the catalyst active sites and the capacitance of the double layer, respectively. R_4 and L_1 stand for the intermediate adsorbate resistance [19]. According to the kinetic theory derived by Harrington and Conway [20] for reactions involving intermediate adsorbate, the Faradaic current in the electrode process of methanol electro-oxidation depends on the electrode potential and one other state variable θ_{CO}, which varies with electrode potential. The inductance L_1 is characteristic of this equivalent circuit and thus deserves an explanation with respect to its mechanistic significance. Inductive behavior means that the current signal follows a voltage perturbation with a phase delay ($\varphi = 90\,^{\circ}C$ for a pure inductor). In the DMFC anode, an increase in potential is obviously followed by an increase in current with a phase delay. This inductive behavior can be rationalized by postulating slowness of CO coverage relaxation. Fig. 8(b) gives the measured EIS values and fitted curves. The dotted-symbols represent the measured values. It can be seen that the impedance results can be well fitted by the equivalent circuit showed in Fig. 8(a). All the fitted resistance parameters of different electrodes are listed in Table 1. MEA with RE exhibits the lowest resistance, while MEA with BE deliver the highest resistance. The smallest resistance of the RE can be ascribed to the good interface property between the catalyst layer and Nafion membrane and the thin catalyst layer. The good interfacial contact between electrode and electrolyte membrane can be obtained due to the relative smooth surface and less cracks of the catalyst layer. Moreover, the contact between the catalyst particles and also between the catalyst particles and the carbon cloth substrate is strengthened when the SE anode is converted to the RE anode.

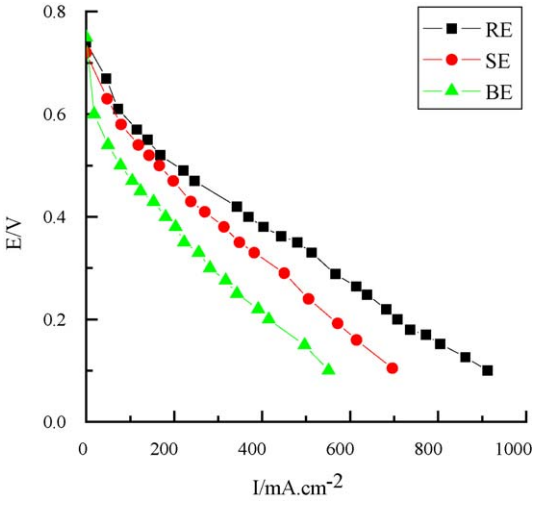

Fig. 9. Current density-cell potential plot of DMFC with different anodes.

It is also feasible to improve the performance of the BE electrode by the treatment with the same process as the SE. Thus, the interfacial resistance of the MEA with RE including diffusion resistance (R_2) charge-transfer resistance (R_3) and the intermediate adsorbate resistance (R_4) is lowest among the three types of MEA.

Fig. 9 shows the polarization curves of MEAs with different anodes as a single direct methanol fuel cell. It can be obviously observed that the single DMFC with the RE delivers the best performance. When the current density is $400\,mA\,cm^{-2}$, the cell voltage for the RE, SE and BE are 0.38, 0.32 and 0.21 V, respectively. The peak power for the single cell with anode RE is about $178\,mW\,cm^{-2}$, while it is $130\,mW\,cm^{-2}$ for the SE and $87\,mW\,cm^{-2}$ for the BE, respectively.

4. Conclusion

Three kinds of anode were made by different process, and their microstructure of catalyst layer was observed by SEM images. The RE had a relative smooth surface and the less cracks than that of SE and the BE. PIXE images revealed that platinum and ruthenium were not dispersed uniformly on the catalyst layer of electrode in the magnitude of micron, and agglomerate catalyst particles formed island-shape rich platinum and ruthenium region. SECM result showed a visual image for catalytic activity distribution of anode, which was consistent with that of PIXE. EIS exhibited that the resistance of the MEA with the RE was the smallest due to the good interfacial contact and the compact catalyst layer. The current density–voltage curves of the single DMFC with different anodes displayed that the MEA with the RE delivered the best discharge performance, and its peak power was $178\,mW\,cm^{-2}$ when the single cell was operating with $2\,mol\,L^{-1}$ methanol solution and 1 bar oxygen gas as oxidant at $70\,^{\circ}C$.

Acknowledgements

The authors gratefully acknowledge ESKOM and NRF for financial support.

References

[1] A. Oliveira Neto, E.G. Franco, E. Arico, M. Linardi, E.R. Gonzalez, J. Eur. Ceram. Soc. 23 (2003) 2987–2992.
[2] T. Okada, Y. Suzuki, T. Hirose, T. Ozawa, Electrochim. Acta 49 (2004) 385–395.
[3] K.-W. Park, J.-H. Choi, S.-A. Lee, C. Pak, H. Chang, Y.-E. Sung, J. Catal. 224 (2004) 236–242.
[4] E. Drioli, A. Regina, M. Casciola, A. Oliveti, F. Trotta, T. Massari, J. Membr. Sci. 228 (2004) 139–148.
[5] V.S. Silva, B. Ruffmann, H. Silva, Y.A. Gallego, A. Mendes, L.M. Madeira, S.P. Nunes, J. Power Sources 140 (2005) 34–40.
[6] Y.-J. Leng, X. Wang, I.-M. Hsing, J. Electroanal. Chem. 528 (2002) 145–152.
[7] A. Pozio, M. De Francesco, A. Cemmi, F. Cardellini, L. Giorgi, J. Power Sources 105 (2002) 13–19.
[8] L.S. Sarma, T.D. Lin, Y.-W. Tsai, J.M. Chen, B.J. Hwang, J. Power Sources 139 (2005) 44–54.
[9] Z. Wei, S. Wang, B. Yi, J. Liu, L. Chen, W. Zhou, W. Li, Q. Xin, J. Power Sources 106 (2002) 364–369.

[10] X. Zhao, X. Fan, S. Wang, S. Yang, B. Yi, Q. Xin, G. Sun, Int. J. Hydrogen Energy 30 (2005) 1003–1010.
[11] Y.-H. Chu, Y.G. Shul, W.C. Cho, S.I. Woo, H.-S. Han, J. Power Sources 118 (2003) 334–341.
[12] N. Nakagawa, Y. Xiu, J. Power Sources 118 (2003) 248–255.
[13] J.-H. Kim, H.Y. Ha, I.-H. Oh, S.-A. Hong, H.-I. Lee, J. Power Sources 135 (1/2) (2004) 29–36.
[14] A.R. Kucernak, P.B. Chowdhury, C.P. Wilde, G.H. Kelsall, Y.Y. Zhu, D.E. Williams, Electrochim. Acta 45 (2000) 4483–4491.
[15] T. Kallio, C. Slevin, G. Sundholm, P. Holmlund, K. Kontturi, Electrochem. Commun. 5 (2003) 561–565.
[16] J. Zhou, Y. Zu, A.J. Bard, J. Electroanal. Chem. 5 (2003) 561–565.
[17] S. Song, G. Wang, W. Zhou, G.Q. Sun, Q. Xin, V. Stergiopoulos, P. Tsiakaras, J. Power Sources 140 (2005) 103–110.
[18] F. Liu, C. Wang, Electrochim. Acta 50 (2005) 1413–1422.
[19] J.T. Müller, P.M. Urban, W.F. Hölderrich, J. Power Sources 84 (1999) 157–160.
[20] D.A. Harrington, B.E. Conway, Electrochim. Acta 32 (1987) 1703–1712.